AGU ADVANCING EARTH AND SPACE SCIENCE

Earth's Future

RESEARCH ARTICLE
10.1029/2022EF002881

Extratropical Climate Change During Periods Before and After an Arctic Ice-Free Summer

Yongkun Xie[1], Hanbin Nie[1,2], and Yongli He[2]

[1]Collaborative Innovation Center for Western Ecological Safety, Lanzhou University, Lanzhou, China, [2]College of Atmospheric Sciences, Lanzhou University, Lanzhou, China

Key Points:

- Seasonality of Arctic warming will change after ice-free relative to that before, under both the intermediate and high future emissions
- Capacitor effect of the Arctic Ocean due to cross-season energy cycle is crucial for seasonality in Arctic climate change
- Arctic amplification induces a decrease in weather variability in mid-high latitudes, especially after ice-free under high emission

Supporting Information:

Supporting Information may be found in the online version of this article.

Correspondence to:

Y. Xie,
xieyk@lzu.edu.cn

Citation:

Xie, Y., Nie, H., & He, Y. (2022). Extratropical climate change during periods before and after an Arctic ice-free summer. *Earth's Future*, *10*, e2022EF002881. https://doi.org/10.1029/2022EF002881

Received 30 APR 2022
Accepted 25 JUL 2022

Abstract The temperature of a well-mixed ice-water mixture stays constant until the ice melts due to external heat. Whether the temperature over the Arctic Ocean exhibits an analogous stagewise evolution to reach an ice-free point remains unclear. Therefore, this study explored the characteristics of extratropical climate change before and after a period during which the Arctic Ocean was ice-free in summer using multimodel simulations. Here, we show that the seasonality of Arctic warming varies between the two periods separated by an ice-free summer. The warming maximum in the cold season delayed for a month after becoming ice-free than before. In addition, the warming maximum lagged behind the sea-ice decline maximum before becoming ice-free, whereas the maximums of the two became coordinated after becoming ice-free. The closed cross-season energy cycle demonstrated that the capacitor effect of the Arctic Ocean with delayed release of the energy taken up in spring and summer due to sea-ice decline and seawater absorption is crucial for the seasonality observed in Arctic climate change. Moreover, we found that although Arctic amplification induced general weakening in high-frequency weather variability in the mid-high latitudes via decreased meridional temperature gradients, significant weakening was induced only after becoming ice-free under high emission. Our findings suggest that the two stages of Arctic sea-ice decline should be taken into consideration when dealing with global warming.

Plain Language Summary Taking the classic stagewise temperature evolution of ice-water mixtures into consideration (Figure S1 in Supporting Information S1), this study investigated climate change in the Arctic before and after an ice-free summer using multimodel simulations. Our results showed that the seasonality characteristics of Arctic warming varied between these two periods. The capacitor effect (charging and discharging in the warm and cold seasons, respectively) of the cross-season energy cycle associated with sea-ice decline on Arctic warming was observed. Moreover, our findings indicated that variability in the weather decreased in mid-high latitudes due to Arctic amplification-induced southward cold airflow from the Arctic not being as cold as before. This research highlights the importance of stagewise decline of Arctic sea-ice.

1. Introduction

Regardless of some discrepancies that exist between them, the multimodel simulations of the Coupled Model Intercomparison Project Phase 5 (CMIP5, Taylor et al., 2012) and 6 (CMIP6, Eyring et al., 2016) predict that Arctic summers will become ice-free during the 21st century (Docquier & Koenigk, 2021; Liu et al., 2013; Notz & Stroeve, 2018; SIMIP Community, 2020; Stroeve et al., 2012; Wang & Overland, 2012). In particular, a practically sea-ice free September, that is a sea-ice area below one million km^2, is predicted to appear for the first time before 2050 under both low and high emission scenarios (shared socioeconomic pathways, SSP; O'Neill et al., 2017) by a majority of CMIP6 models (SIMIP Community, 2020). In addition, a sea-ice free summer would arrive in the 2030s according to both CMIP5 and CMIP6 when these models were selected based on observations (Docquier & Koenigk, 2021; Wang & Overland, 2012). Irrespective of the time by which an ice-free summer will appear, an adequate understanding of an ice-free period and related climate change characteristics is felt to be needed.

Arctic warming shows prominent seasonality. Observations demonstrated that amplification of Arctic warming has been strongest in the cold seasons during the past several decades (Screen & Simmonds, 2010; Serreze & Francis, 2006; Stouffer & Manabe, 2017). This seasonality was also demonstrated by the future projections of the climate models (Holland & Bitz, 2003; Lu & Cai, 2009; Manabe & Stouffer, 1980; Pithan & Mauritsen, 2014).

By contrast, sea-ice decline in the Arctic is greatest in the summer (Notz & Stroeve, 2016; Serreze et al., 2007). These findings demonstrated that the changes in sea-ice and temperature in the Arctic are roughly out-of-phase across seasons. Previous studies have proposed that sea-ice decline accompanied by albedo feedbacks (Crook et al., 2011; Dai et al., 2019; Screen & Simmonds, 2010; Xie et al., 2019), longwave radiation feedbacks associated with the moisture of atmosphere and clouds (Francis et al., 2005; Kapsch et al., 2013; Lu & Cai, 2009; Pithan & Mauritsen, 2014; Screen, 2017; Taylor et al., 2013; Winton, 2006), and poleward oceanic and atmospheric energy transport (Delworth et al., 2016; Graversen & Burtu, 2016; Tsubouchi et al., 2021; Zhang et al., 2008; Årthun et al., 2019), are all factors that may be associated with seasonality in Arctic warming.

The effect of sea-ice decline in the summer on delayed warming in the winter may be linked to energy-uptake and -release processes between the Arctic Ocean and the atmosphere (Dai et al., 2019; Laîné et al., 2016; Screen & Simmonds, 2010; Xie et al., 2019; Yoshimori et al., 2017). However, some studies have suggested that summertime sea-ice decline plays only a minor role during wintertime Arctic warming amplification (Gao et al., 2019; Lu & Cai, 2009). Multimodel simulations may help further clarify this issue. As elaborated in Section 3, the magnitudes and seasonality of sea-ice decline vary among cases. Therefore a comparison between the two periods that are separated by an ice-free summer under various future scenarios may demonstrate the effects of sea-ice. This approach is based on the "natural experiment" concept (Ball, 2021). The primary benefit of this approach relative to the "prescribed-forcing" type experiments, such as prescribed-sea ice experiments proposed in the polar amplification MIP (PAMIP, Smith et al., 2019) of CMIP6, is that multisphere interactions are not restricted. The fully active multisphere interactions are crucial for Arctic climate change-related investigations. For example, multisphere interactions are suggested to be the most relevant to the Arctic and mid-latitude connections (Blackport et al., 2019; Xie et al., 2021). Thus, comparisons between the two periods before and after an ice-free summer may be helpful.

In addition, previous studies have suggested that more extreme cold weather events may occur under amplified Arctic warming due to anomalous atmospheric circulation (Cohen et al., 2018; Francis & Vavrus, 2012; Honda et al., 2009; Huang et al., 2017; Overland et al., 2016; Wang et al., 2020; Wu et al., 2016). However, studies have also proposed that amplified Arctic warming may result in fewer cold extremes due to synoptic cold temperature advection becoming weak, which occurs when meridional temperature gradients become weak (Blackport et al., 2022; Schneider et al., 2015). Consequently, ultra-changes in extratropical weather depend on a combination of dynamical (changes in circulation) and thermal (changes in temperature gradients) effects (Overland et al., 2016; Screen, 2017). Therefore, multimodel simulations that verify these dynamical and thermal effects by investigating changes in weather variability is warranted.

By investigating climate change during the two periods before and after an ice-free summer under different future scenarios, this study may help gain further insights into the seasonality of Arctic warming, the effects of sea-ice decline, and changes in extratropical weather under Arctic amplification. Multimodel simulations from historical as well as SSP-based future simulations of CMIP6 were examined in this paper. The historical and representative concentration pathways (RCP)-based future simulations of the CMIP5 were also examined to verify CMIP6 results. The results of those two generations of CMIP models were found to be consistent. The remainder of this paper is organized in five parts. Data and methods are introduced in Section 2. Characteristics of the projected changes in temperature and sea-ice in the Arctic are addressed in Section 3. Section 4 elaborates on the causes of variable seasonality in Arctic warming during the two stages of Arctic sea-ice decline. Projected changes in high-frequency weather variability are demonstrated in Section 5. Conclusions and discussion are presented in Section 6.

2. Data and Methods

Thirty-one CMIP6 and five CMIP5 models used in this study are shown in Tables S1 and S2 in Supporting Information S1, respectively. The variables from model outputs that were examined are listed in Table S3 in Supporting Information S1. All CMIP6 models that the required variables are available were selected. To select the CMIP5 models, only five models that best simulated the historical Arctic sea-ice evolution and had an ice-free summer near the 2050s, according to Wang and Overland (2012), were used. In addition, in cases where more than three ensemble members of CMIP6 simulations were available, only the first three were used (Table S1 in Supporting Information S1), whereas all ensemble members of CMIP5 simulations were used (Table S2 in

Supporting Information S1). Before calculating the multimodel ensemble means and corresponding standard deviations, the ensemble members of each single model were averaged, in order to impart equal weight to each model. Before plotting the spatial map of the multimodel ensemble mean, CMIP6 and CMIP5 simulations were bilinearly interpolated into a 1.0° by 1.0° and 1.5° by 1.5° grid, respectively.

Three sets of CMIP6 experiments, involving one historical and two future projection experiments on intermediate (SSP245) and high (SSP585) emissions (Eyring et al., 2016; O'Neill et al., 2017), were examined in this study. The CMIP6 historical and future projection experiments cover the period from 1850 to 2014 and from 2015 to 2100, respectively. In addition, two sets of CMIP5 historical and high-emission future projection (RCP8.5) experiments (Taylor et al., 2012) were used in this study. The CMIP5 historical and future projection experiments cover the period from 1850 to 2005 and from 2005 to 2100, respectively. These historical and future projection simulations were merged to obtain a continuous time series from 1850 to 2100. All variables examined were monthly means, except for near-surface air temperature (SAT) which was examined in both monthly and daily means (Table S3 in Supporting Information S1). Daily SAT data were used to investigate high-frequency weather variability.

Sea-ice area (SIA) was calculated using sea-ice concentration (SIC) multiply by cell areas of the ocean or atmosphere grids from CMIP6 (Table S3 in Supporting Information S1, SIMIP Community, 2020). Local energy budget at earth surface (Xie et al., 2019) was examined to elucidate the causes of the seasonality of Arctic warming. Net energy uptake at earth surface equals the sum of net shortwave ($\text{Net\_SW}\downarrow = \text{SW}\downarrow - \text{SW}\uparrow$) and longwave ($\text{LW}\downarrow - \text{LW}\uparrow$) radiation minus the sum of upward sensible ($\text{SH}\uparrow$) and latent heat ($\text{LH}\uparrow$), that is $\text{Net\_Energy}\downarrow = \text{Net\_SW}\downarrow + \text{LW}\downarrow - \text{LW}\uparrow - \text{SH}\uparrow - \text{LH}\uparrow$. The linear trend was calculated via linear regression based on the least squares method. The corresponding significance was estimated using the two-tailed Student's t-test. Statistical significance was set at 95% ($P < 0.05$).

High-frequency weather variability was depicted in two ways: standard deviation of the daily SAT; and extremely warm and cold weather events (warm/cold extremes). Standard deviation of the daily SAT was calculated at each grid for each calendar month of each year using daily SAT data. Extreme weather events were defined using two approaches: deviations from a running state (e.g., Xie et al., 2017); or a fixed reference state (e.g., Horton et al., 2015). The procedures adopted for the running reference state-based approach were as follows: (a) reference state means (i.e., 31-day running means) at each grid were calculated using daily SAT data; (b) daily SAT anomalies were calculated by subtracting the reference state means; (c) for each month, all daily SAT anomalies from 2000 to 2100 were considered as a population; and (d) any day with a SAT anomaly located outside the two-tailed 5th percentile (1.96 times of standard deviation; 2.5th percentile on each side) was identified as an extreme weather event.

The four-step procedures that were adopted for a fixed reference state-based approach were similar, except for the fact that the reference state means in the first step were directly calculated as the climatological monthly mean for 2000–2100. In the running reference state-based approach, variation in the reference state means was ejected. By contrast, the fixed reference state-based approach directly contains the signals of the variation in monthly mean SAT. Consequently, the trends shown by identified extreme weather events were largely manifestations of the trends in monthly mean SAT. For example, the cold (warm) extremes would become less (more) due to an increase in mean SAT (Figures S9 and S10 in Supporting Information S1). This indicates that the fixed reference state-based approach has substantial limitations in depicting high-frequency weather variability for the purposes of this study. Therefore, these extreme weather events were quantified according to a running reference state-based approach, as described in Section 5.

3. Projected Changes in Temperature and Sea-Ice in the Arctic

Changes in temperature and sea-ice before the 1980s were minor (Figure 1 and Figure S2 in Supporting Information S1), indicating that climate changes in the Arctic were not evident before the 1980s. After the 1980s, increase in temperature and decline in sea-ice were enhanced. The magnitudes of changes varied across seasons (Figure 1). The magnitudes of temperature increase were stronger in the cold season than those in the warm season, under both intermediate and high emissions (Figures 1a and 1b). By contrast, the relative magnitudes of sea-ice decline across seasons varied with periods. With due consideration to the properties of ice-water mixture (Figure S1 in Supporting Information S1), this study examined the changes that occurred during two periods

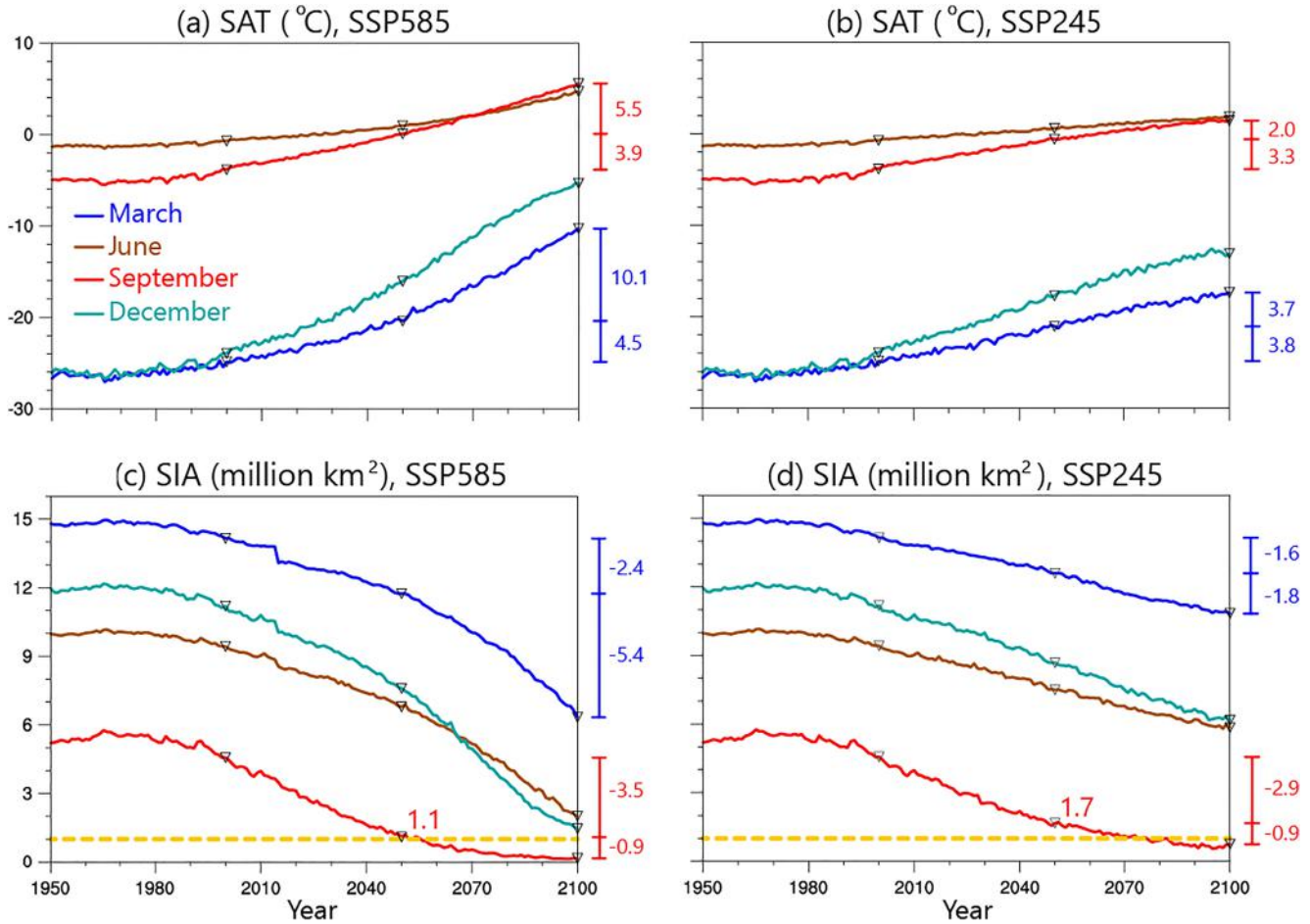

Figure 1. Time series of the monthly mean near-surface air temperature (surface air temperature (SAT); top) and sea-ice area (Sea-ice area (SIA); bottom) in the Arctic from 1950 to 2100. The results show multimodel ensemble means based on the combination of historical and shared socioeconomic pathways (SSP585) (left) or SSP245 (right) simulations from coupled model intercomparison project Phase 6 (CMIP6) (Section 2), respectively. SAT was averaged over 70°N poleward, while SIA was the sum across the Northern Hemisphere. The bars and numbers on the right depict values in 2000, 2050, and 2100 (marked by inverted triangles) and the increments from 2000 to 2050 and from 2050 to 2100, respectively. The yellow lines in (c and d) indicate the threshold of 1 million km^2, which is the criterion for being practically sea-ice free. Uncertainty in the multimodel results and the CMIP5 results are shown in Figure S2 in Supporting Information S1.

divided by a practically ice-free summer. The ice-free summer (September, sea-ice minimum month of the year) is predicted to occur around 2050 under high emission (Figure 1c), whereas the ice-free point arrives around 2070 under intermediate emission (Figure 1d). In fact, the September SIA of 1.7 million km^2 in 2050 will be at a substantially low level relative to the ~5 million km^2 that was present before the 1980s (Figure 1d). Therefore, for the purpose of a better comparison, the ice-free demarcation point was selected as 2050 for both intermediate and high emissions (SIMIP Community, 2020). Before the ice-free summer (2000–2050), the magnitudes of sea-ice decline were stronger in September than in March (sea-ice maximum of the year) under both intermediate and high emissions (Figures 1c and 1d). By contrast, the magnitudes of sea-ice decline are stronger in March than that in September after the ice-free summer (2050–2100).

The seasonalities in Arctic warming and sea-ice decline during the periods before and after the ice-free are shown in Figure 2. A general out-of-phase relation between the magnitudes of Arctic warming and sea-ice decline was prominent during the two periods under both intermediate and high emissions. However, the specific seasonalities of Arctic warming and sea-ice decline during these two periods were different. Before becoming ice-free, the 3 months with the maximum sea-ice decline were September, October, and November under high emission, whereas maximum warming occurred 2 months later than the sea-ice decline (Figure 2a). Maximum warming lagged 1 month behind sea-ice decline under intermediate emission (Figure 2c). By contrast, the maximums of both sea-ice decline and warming under both intermediate and high emissions became coordinated during

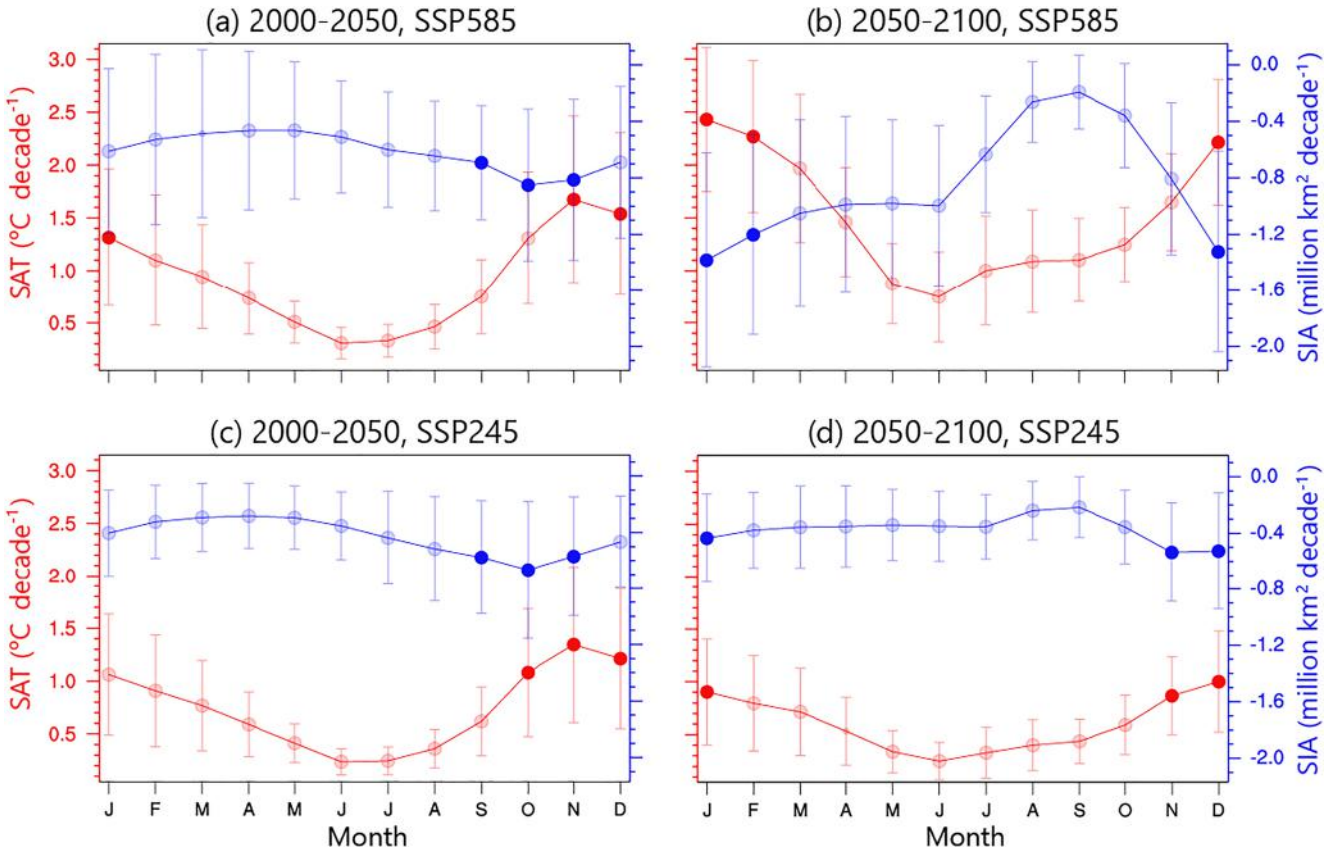

Figure 2. Linear trends in the monthly mean surface air temperature (SAT) (red) and Sea-ice area (SIA) (blue) in the Arctic for 2000–2050 (left) and 2050–2100 (right), respectively. The top and bottom panels are based on a combination of historical and shared socioeconomic pathways (SSP585) or SSP245 simulations, respectively. The large dot indicates that the linear trend is significant at the 95% confidence level based on a two-tailed Student's *t*-test. Vertical bars represent the range of one standard deviation of the multimodel results. The three dots of deeper color indicate the 3 months with the largest magnitudes of warming or sea-ice decline.

the period after becoming ice-free (Figures 2b and 2d). In addition, maximum sea-ice decline occurred two (Figures 2c and 2d) and three (Figures 2a and 2b) months later after becoming ice-free than before, under intermediate and high emissions, respectively. Maximum warming occurred 1 month later after becoming ice-free than before (Figure 2). Since each season includes 3 months, the results demonstrated that the seasonalities in Arctic warming and sea-ice decline have changed after becoming ice-free than before, regardless of whether these changes were one or 3 months. In particular, high emission induced a stronger sea-ice decline in summer and a longer delay in the warming maximum during the period before becoming ice-free, than did intermediate emission (Figures 2a and 2c). The effects of summertime sea-ice decline on lagged wintertime Arctic warming, and the underlying mechanisms will be elaborated on in the next section. Note that these conclusions were consistent with those of CMIP5 results (Figures S2 and S3 in Supporting Information S1).

4. Causes of the Varied Seasonality in Arctic Warming During the Two Periods

The local energy budget (Section 2) at the earth surface was examined to clarify the mechanisms underlying seasonality in Arctic warming (Figures 3 and 4). Net shortwave radiation increase was strongest in summer (Figure 3) due to the combined effects of sea-ice decline and strong solar incidence in summer (polar nights in winter). However, strongest net shortwave radiation (Figure 3) corresponded to the weakest rather than the strongest warming in summer (Figure 2). Therefore, shortwave radiation uptake by the Arctic Ocean is not released immediately via longwave radiation and sensible/latent heat, and induces a lagged net energy cycle across seasons (Figure 4). As per the Stefan-Boltzmann law, longwave feedback synchronized upward and downward longwave radiation with Arctic warming, during each month of the year (Figures 2–4 and Figure S4 in Supporting Information S1; Dai et al., 2019; Pithan & Mauritsen, 2014; Xie et al., 2021). Therefore, downward longwave radiation

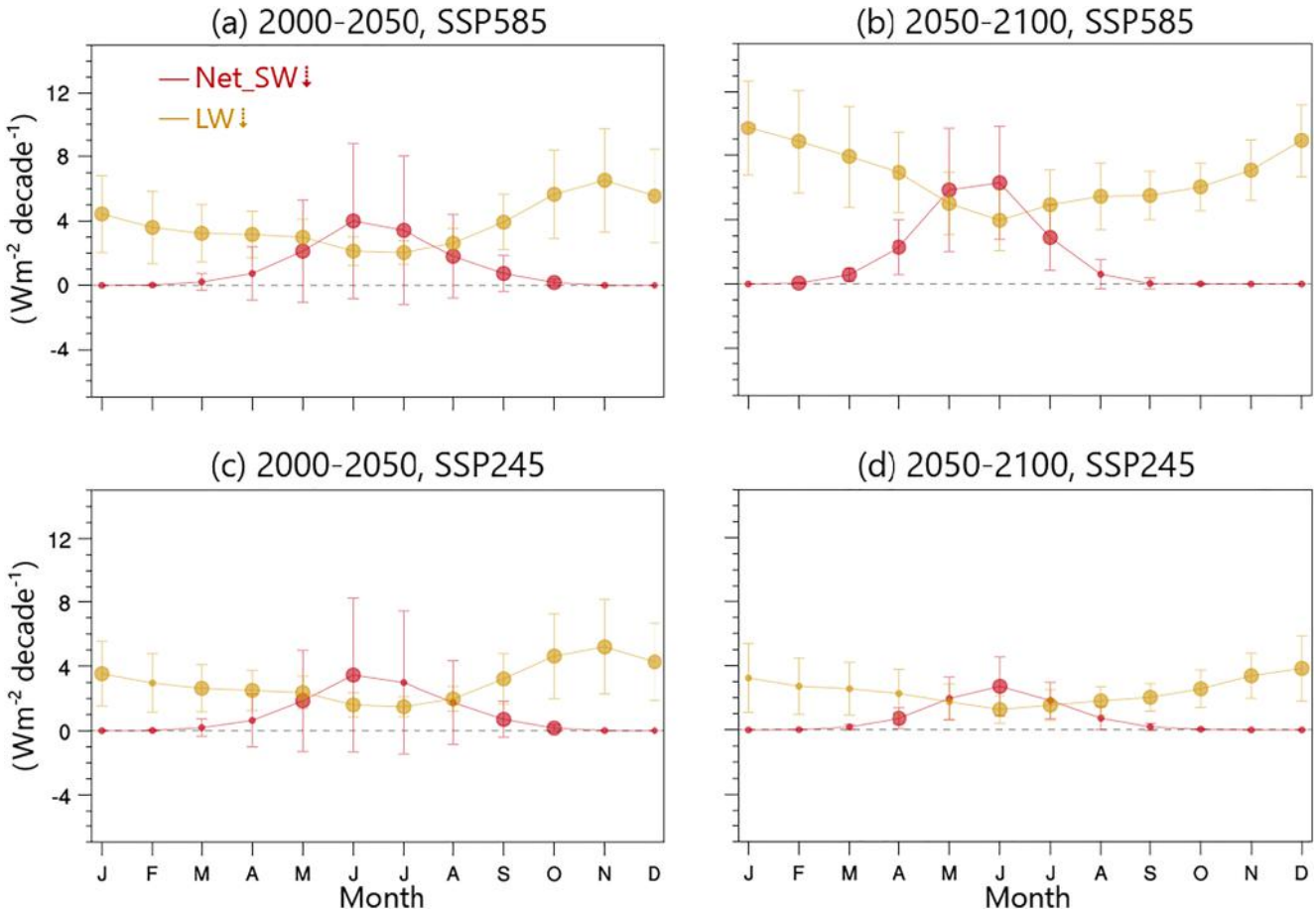

Figure 3. Same as Figure 2 but for linear trends in net shortwave radiation (Net_SW↓, red, Section 2) and downward longwave radiation (LW↓, gold) in the Arctic (averaged over the 70°N poleward).

appears to be the dominant factor that directly induces seasonality in Arctic warming (Figures 2 and 3), especially in clear-sky situations (Gao et al., 2019; Lu & Cai, 2009). However, the effects of the cross-season energy cycle on the seasonality in Arctic warming appear to play an essential role (Figure 4), as elaborated in the next section.

Both summertime net energy uptake and wintertime net energy release through the surface of the Arctic Ocean were prominent (Figure 4). A vanished annual mean net energy indicates that the cross-season energy cycle was closed, which is analogous to the charging-discharging cycle of the battery, that is, the capacitor effect of ocean (Xie et al., 2009). Net shortwave radiation dominated the increase in net energy uptake in spring and summer (Figures 3 and 4). Upward longwave radiation and sensible and latent heat jointly released the uptaken energy in winter (Figures 3 and 4, and Figure S4 in Supporting Information S1). Longwave radiation and sensible heat are directly related to temperature, whereas latent heat affects temperature via the phase transformation of water vapor. In addition to these general characteristics, varied seasonalities in energy budget trends may explain varied seasonality in Arctic warming during these two periods.

Under continuous warming, annual melting and freezing times arrive earlier and later, respectively. Therefore, energy uptake time through net shortwave radiation associated with sea-ice decline and seawater came earlier during the period after becoming ice-free than before (Figure 3). During the period before becoming ice-free, there was a significant (95% confidence level) increase in shortwave radiation spanning May to October under intermediate and high emissions (Figures 3a and 3c). The significant increase in shortwave radiation started 3 months and 1 month earlier during the period after becoming ice-free (Figures 3b and 3d) than those before (Figures 3a and 3c). Since the quantity of sea-ice is limited in summer, the significant increase in shortwave radiation due to the decline in sea-ice decline also ended earlier during the period after becoming ice-free than before (Figure 3). These results demonstrated that sea-ice decline in spring and summer (Figure 2) was crucial

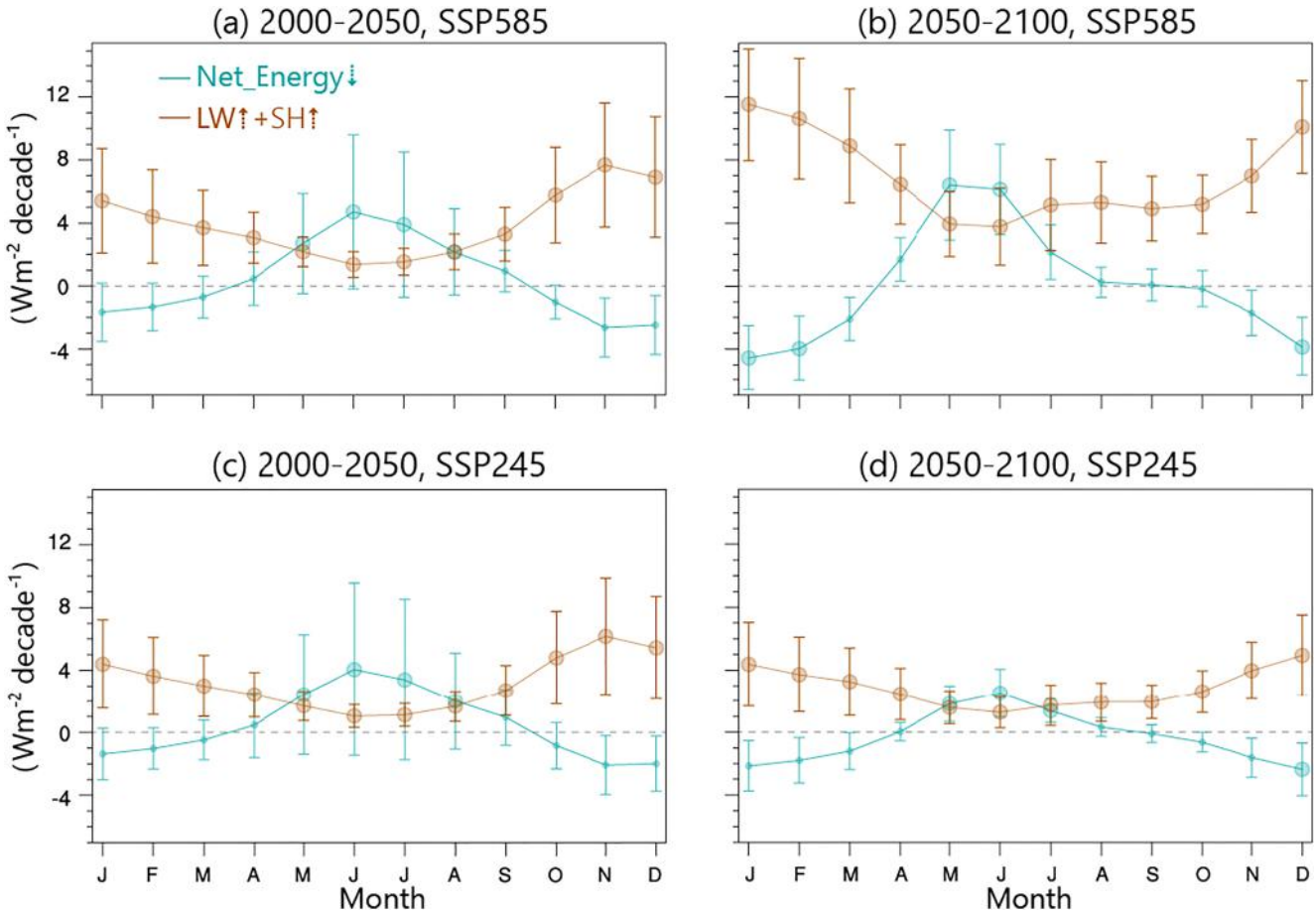

Figure 4. Same as Figure 3 but for net energy uptake (Net_Energy↓ = Net_SW↓ + LW↓ − LW↑ − SH↑ − LH↑, turquoise, Section 2) and the sum of upward longwave radiation and sensible heat (LW↑ + SH↑, bronze). The corresponding results for individual LW↑, SH↑, and LH↑ are shown in Figure S4 in Supporting Information S1.

for the cross-season energy cycle (Figures 3 and 4). In addition, the energy release (via phase change of seawater) time was delayed after becoming ice-free than before, due to delayed freezing time (Figure 4). Consequently, the warming maximum occurred later after becoming ice-free (Figure 2). Therefore, altered freezing time was responsible for the delayed warming maximum during the period after becoming ice-free than before, whereas altered freezing time and limited sea-ice (for melting) in summer jointly induced varied relationships between the maximums of sea-ice decline and warming during the two periods. Conclusions concerning the energy budget were supported by CMIP5 results (Figure S3 in Supporting Information S1). However, the specific processes that were active within the subsurface ocean during the period extending from the summertime energy uptake to wintertime energy release need further investigation.

5. Projected Changes in Weather Variability

In addition to the monthly mean climate, changes in high-frequency weather variability were also explored. One standard deviation of daily temperature and identified extreme weather events (running reference state-based approach, Section 2) were used to depict high-frequency weather variability. Linear trends in the one standard deviation of daily temperature decreased for both mid-high latitudes (30°–70°N) and Arctic (70°–90°N) across the year except for summer (Figure 5). During the period before becoming ice-free, the decrease in weather variability in the Arctic was significant (95% confidence level) only for the months from September to November (Figures 5a and 5c), although the decreased weather variability occurred in most months in both mid-high latitudes and the Arctic. This significant decrease in weather variability in the Arctic was related to the maximum sea-ice decline that occurred during the 3 months from September to November (Figures 2a and 2c). Under high emission, the decrease in the weather variability in the Arctic became stronger during the period after becoming

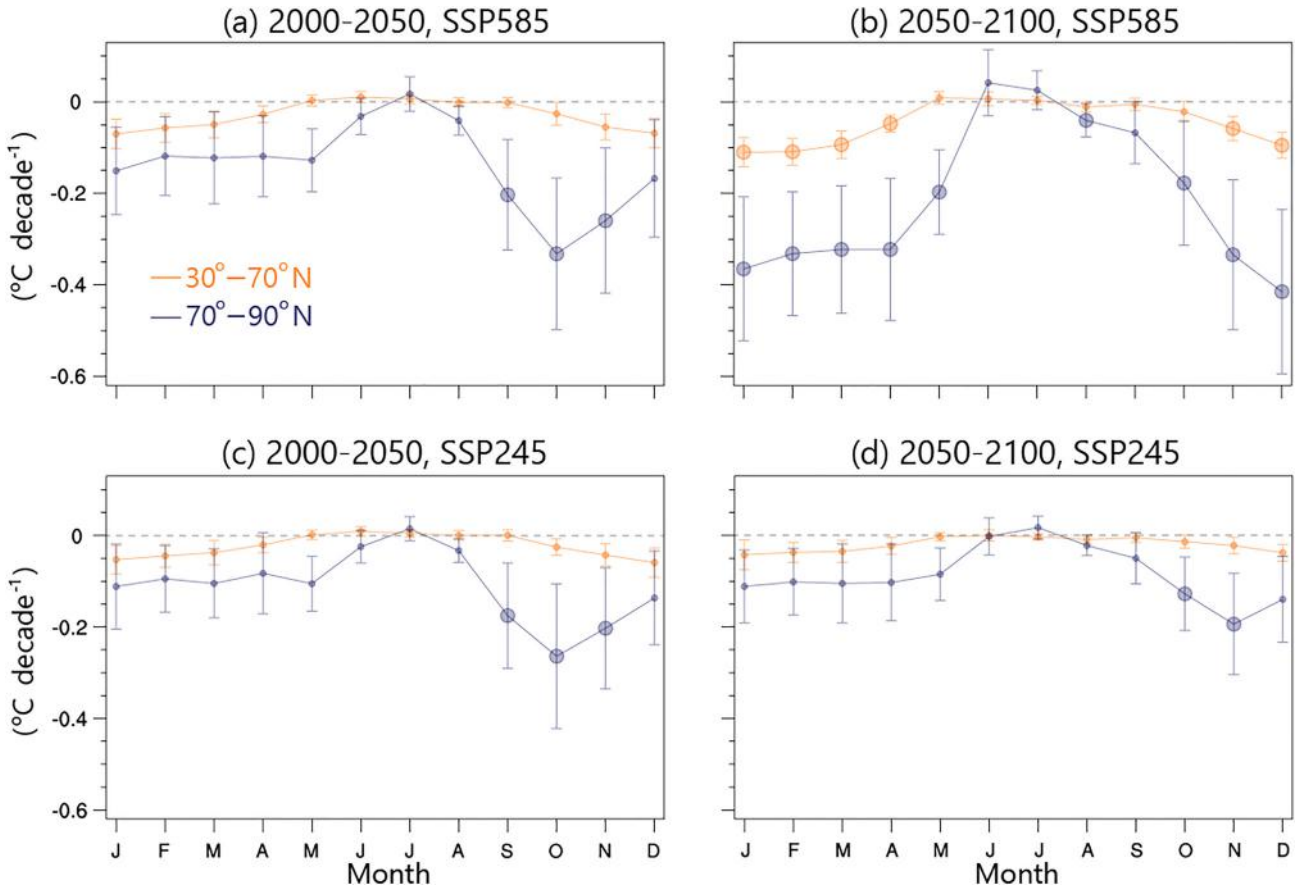

Figure 5. Linear trends in one standard deviation of daily surface air temperature in each month (Section 2) in the mid-high latitudes (30°–70°N; orange) and Arctic (70°–90°N; cool gray) for 2000–2050 (left) and 2050–2100 (right), respectively. The top and bottom panels depict results based on the combination of historical and shared socioeconomic pathways (SSP585) or SSP245 simulations, respectively. The large dots indicate that the linear trend is significant at the 95% confidence level, based on a two-tailed Student's *t*-test. Vertical bars represent one standard deviation range of the multimodel results. The corresponding spatial distributions are presented in Figure 6 and Figure S5 in Supporting Information S1.

ice-free than before (Figures 5a and 5b), which was also related to a stronger sea-ice decline (Figures 2a and 2b). In addition, the regions showing a larger decrease in weather variability (Figure 6) were the regions with a stronger sea-ice decline (not shown), indicating that the decrease in weather variability over the Arctic Ocean may be attributed to sea-ice decline. Sea ice-covered ocean is thrown open when much of the sea ice melts. Consequently, high-frequency temperature variability over the open ocean becomes weaker than that over the sea-ice owing to the heat capacity of seawater being greater than that of sea-ice. This was demonstrated by the climatology of high-frequency weather variability distribution, wherein weather variability over land and sea-ice regions was larger than that over the ocean (not shown).

Although a decrease in weather variability occurred in most months under both intermediate and high emissions, a significant decrease in the weather variability of mid-high latitudes occurred only in the cold season after becoming ice-free under high emission (Figure 5b). This significant change (Figure 5b) may be attributed to Arctic warming becoming the strongest during the period after becoming ice-free under high emission, relative to other cases (Figure 2). When the results of the two periods under intermediate and high emissions were compared, the association between stronger Arctic warming (Figure 2) and the larger decrease in weather variability in mid-high latitudes (Figure 5) was prominent. This suggests that the Arctic amplification-induced decrease in meridional temperature gradients may have reduced weather variability in mid-high latitudes. Pertaining to the dynamic processes involved in cold air outbreaks, Arctic amplification induced the cold air to become less cold than before, thereby weakening temperature advection-induced cooling as well. Moreover, the changes in extreme weather events (Figure 7, Figures S6, and S7 in Supporting Information S1) were consistent with those in one standard deviation of daily temperature (Figures 4 and 5, and S5 in Supporting Information S1). These results

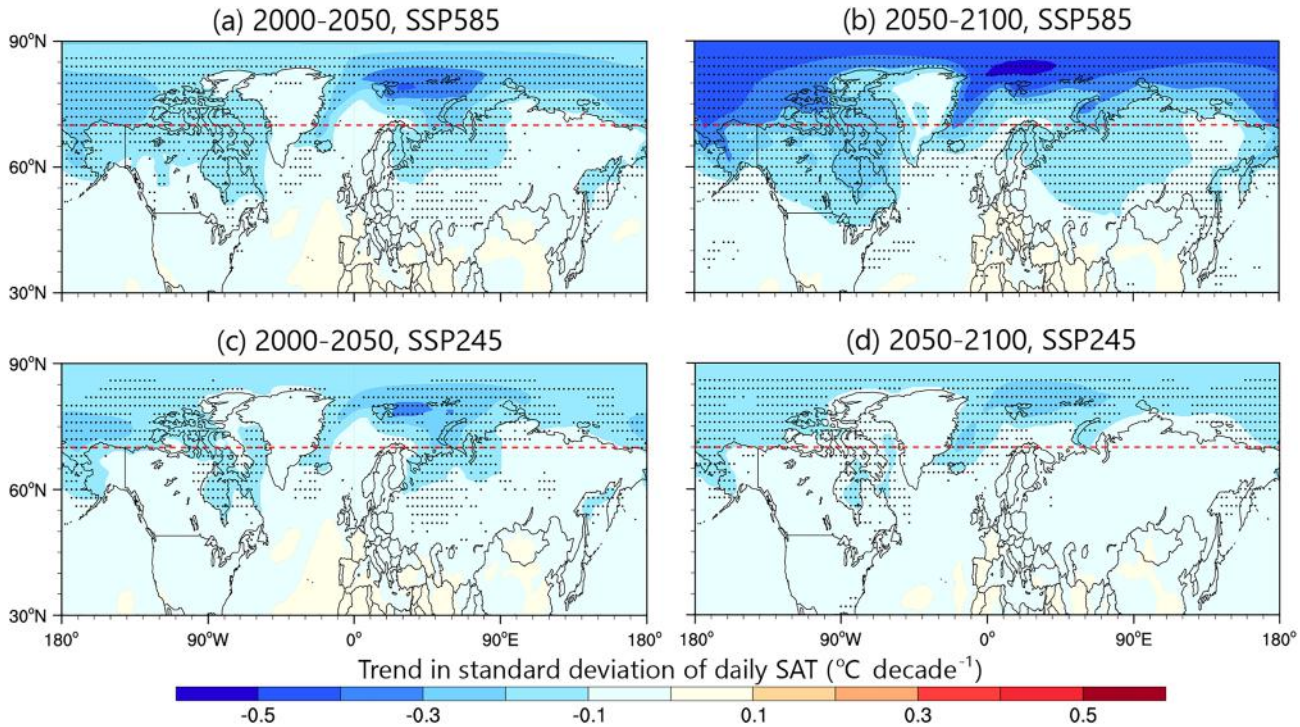

Figure 6. Spatial distribution of the linear trends in one standard deviation of daily surface air temperature for 2000–2050 (left) and 2050–2100 (right), respectively. The results are averaged throughout the year except summer (i.e., January to May and September to December). The top and bottom panels depict results based on the combination of historical and shared socioeconomic pathways (SSP585) or SSP245 simulations, respectively. The dots indicate that more than 95% of the models are consistent in signs. The red line indicates 70°N cutting latitude corresponding to Figure 5.

also substantiated CMIP5 results (Figure S8 in Supporting Information S1). Thus, the thermal effects exerted by changes in the temperature gradients (Blackport et al., 2022; Schneider et al., 2015) of Arctic amplification on weather variability in the mid-high latitudes were verified via multimodel simulations. However, only strong future warming under high emission during the period after becoming ice-free led to statistically significant thermal effect-induced changes (Figures 5–7). In addition, these multimodel simulations demonstrated that dynamical effects (changes in circulation) were minor.

6. Conclusions and Discussion

Using multimodel simulations from CMIP6 and CMIP5, this study demonstrated that seasonality of Arctic warming changed during the period after becoming summer ice-free than the period before it. Changes in seasonality were related to the cross-season energy cycle in the Arctic Ocean, that is, capacitor effect. Warming-induced delayed freezing times caused changes in the cross-season energy cycle. In particular, the delayed release of the energy taken up in spring and summer induced by the decline in sea-ice and absorption of seawater were crucial. Phase differences between the maximums of warming and the decline in sea-ice vanished after becoming ice-free, which was due to the joint effect of the limited quantity of sea-ice in summer and altered freezing time. Our findings further demonstrated that the decline in sea-ice was responsible for decreased high-frequency weather variability over the Arctic Ocean. Moreover, the impact of Arctic amplification on weather variability in the mid-latitudes was dominated by thermal effects associated with temperature gradients rather than by the dynamical effects associated with circulation.

Although the closed cross-season energy cycle was prominent, explicit mechanisms underlying this energy cycle still remain inadequately clarified. In particular, data pertaining to the detailed behavior of energy within the ocean subsurface during the period between its uptake in spring and summer and release in winter are lacking. Further investigations focusing on the energy flow within the ocean subsurface are felt to be required. In addition, investigations may be required to clarify whether multimodel ensemble means have limitations in capturing the

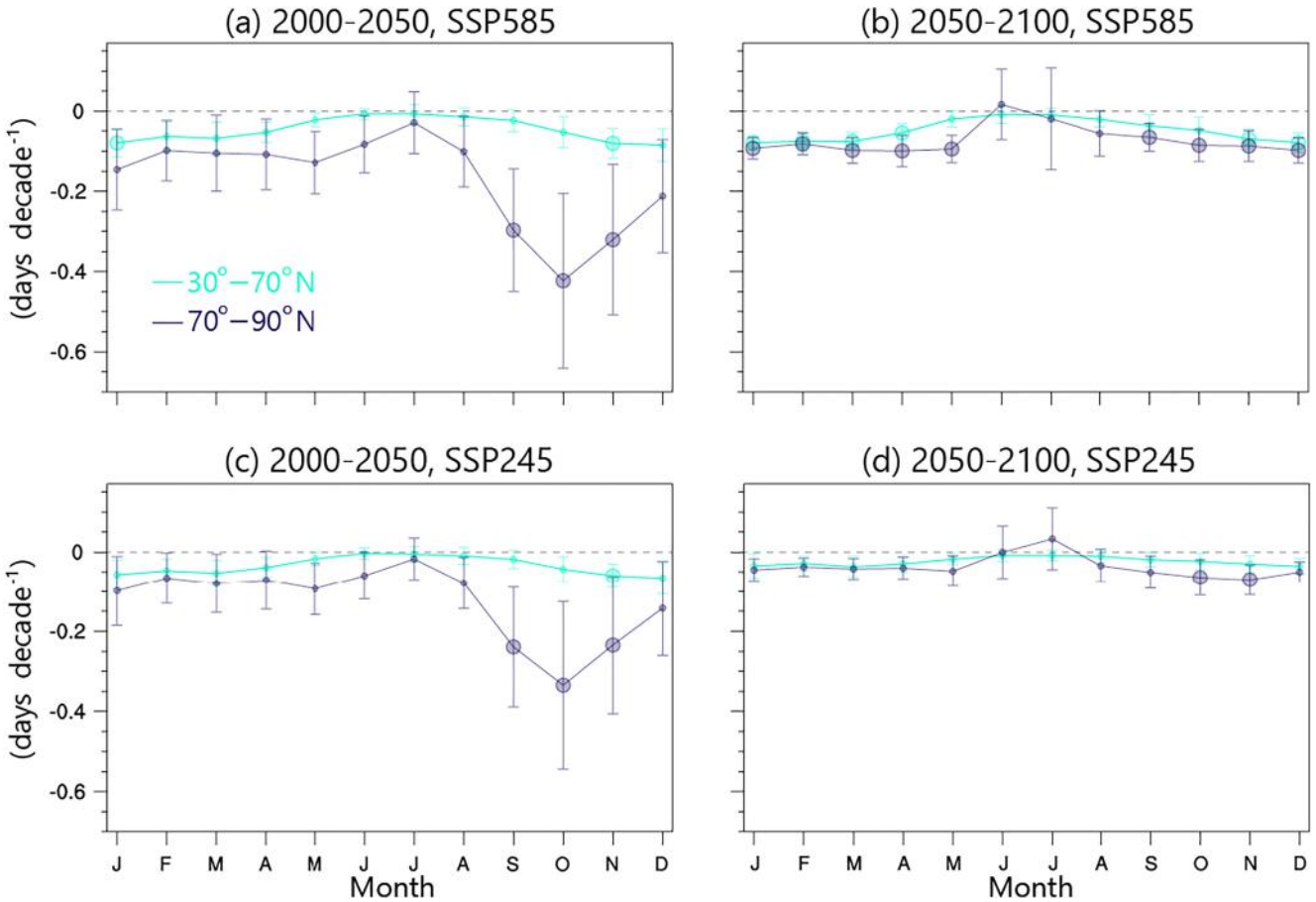

Figure 7. Same as Figure 5 but for the occurrence of the extremely cold days (cold extremes; Section 2). The extreme level is outside the 95% percentile (1.96 times of standard deviation) of the two-tailed normal distribution. The figure for extremely warm days is shown in Figure S6 in Supporting Information S1.

anomalous circulations that contribute to weather variability. For example, dynamically induced variability in the previous warming slowdown was not well captured by most climate models (Guan et al., 2015; Kosaka & Xie, 2013; Steinman et al., 2015). Therefore, some uncertainty remains regarding the magnitude of the dynamical effects of Arctic amplification on weather variability in mid-high latitudes (Blackport et al., 2022; Coumou et al., 2018; Schneider et al., 2015; Screen, 2017). Practically, varied seasonality seen in Arctic climate changes during the two stages of sea-ice decline must be taken into consideration when dealing with continuous global warming in the future.

Data Availability Statement

All the data examined in this study are publicly available on their official websites. The CMIP5 and CMIP6 data are available at https://esgf-node.llnl.gov/search/cmip5/ and https://esgf-node.llnl.gov/search/cmip6/, respectively.

Acknowledgments
We thank anonymous reviewers for constructive and helpful comments. We acknowledge the World Climate Research Programme's Working Group on Coupled Modelling. We are also grateful for the institutes for sharing their model outputs. This work is supported by the National Natural Science Foundation of China (91937302, 42030602) and the Gansu Provincial Special Fund Project for Guiding Scientific and Technological Innovation and Development (2019ZX-06).

References

Årthun, M., Eldevik, T., & Smedsrud, L. (2019). The role of Atlantic heat transport in future Arctic winter sea ice loss. *Journal of Climate*, *32*(11), 3327–3341. https://doi.org/10.1175/jcli-d-18-0750.1

Ball, P. (2021). Nobel-winning 'natural experiments' approach made economics more robust. *Nature*. https://doi.org/10.1038/d41586-021-02799-7

Blackport, R., Fyfe, J. C., & Screen, J. A. (2022). Arctic change reduces risk of cold extremes. *Science*, *375*(6582), 729. https://doi.org/10.1126/science.abn2414

Blackport, R., Screen, J. A., van der Wiel, K., & Bintanja, R. (2019). Minimal influence of reduced Arctic sea ice on coincident cold winters in mid-latitudes. *Nature Climate Change*, *9*, 697–704. https://doi.org/10.1038/s41558-019-0551-4

Cohen, J., Pfeiffer, K., & Francis, J. A. (2018). Warm Arctic episodes linked with increased frequency of extreme winter weather in the United States. *Nature Communications*, *9*(1), 869. https://doi.org/10.1038/s41467-018-02992-9

Coumou, D., Di Capua, G., Vavrus, S., Wang, L., & Wang, S. (2018). The influence of Arctic amplification on mid-latitude summer circulation. *Nature Communications*, *9*(1), 2959. https://doi.org/10.1038/s41467-018-05256-8

Crook, J. A., Forster, P. M., & Stuber, N. (2011). Spatial patterns of modeled climate feedback and contributions to temperature response and polar amplification. *Journal of Climate*, *24*(14), 3575–3592. https://doi.org/10.1175/2011jcli3863.1

Dai, A., Luo, D., Song, M., & Liu, J. (2019). Arctic amplification is caused by sea-ice loss under increasing CO_2. *Nature Communications*, *10*(1), 121. https://doi.org/10.1038/s41467-018-07954-9

Delworth, T., Zeng, F., Vecchi, G., Yang, X., Zhang, L., & Zhang, R. H. (2016). The North Atlantic Oscillation as a driver of rapid climate change in the Northern Hemisphere. *Nature Geoscience*, *9*(7), 509–512. https://doi.org/10.1038/ngeo2738

Docquier, D., & Koenigk, T. (2021). Observation-based selection of climate models projects Arctic ice-free summers around 2035. *Communications Earth & Environment*, *2*(1), 144. https://doi.org/10.1038/s43247-021-00214-7

Eyring, V., Bony, S., Meehl, G. A., Senior, C. A., Stevens, B., Stouffer, R. J., & Taylor, K. E. (2016). Overview of the Coupled Model Intercomparison Project Phase 6 (CMIP6) experimental design and organization. *Geoscientific Model Development*, *9*(5), 1937–1958. https://doi.org/10.5194/gmd-9-1937-2016

Francis, J. A., Hunter, E., Key, J. R., & Wang, X. (2005). Clues to variability in Arctic minimum sea ice extent. *Geophysical Research Letters*, *32*(21), L21501. https://doi.org/10.1029/2005gl024376

Francis, J. A., & Vavrus, S. J. (2012). Evidence linking Arctic amplification to extreme weather in mid-latitudes. *Geophysical Research Letters*, *39*(6), L06801. https://doi.org/10.1029/2012gl051000

Gao, K., Duan, A., Chen, D., & Wu, G. (2019). Surface energy budget diagnosis reveals possible mechanism for the different warming rate among Earth's three poles in recent decades. *Science Bulletin*, *64*(16), 1140–1143. https://doi.org/10.1016/j.scib.2019.06.023

Graversen, R., & Burtu, M. (2016). Arctic amplification enhanced by latent energy transport of atmospheric planetary waves. *Quarterly Journal of the Royal Meteorological Society*, *142*(698), 2046–2054. https://doi.org/10.1002/qj.2802

Guan, X., Huang, J., Guo, R., & Lin, P. (2015). The role of dynamically induced variability in the recent warming trend slowdown over the northern hemisphere. *Scientific Reports*, *5*(1), 12669. https://doi.org/10.1038/srep12669

Holland, M. M., & Bitz, C. M. (2003). Polar amplification of climate change in coupled models. *Climate Dynamics*, *21*(3–4), 221–232. https://doi.org/10.1007/s00382-003-0332-6

Honda, M., Inoue, J., & Yamane, S. (2009). Influence of low Arctic sea-ice minima on anomalously cold Eurasian winters. *Geophysical Research Letters*, *36*(8), L08707. https://doi.org/10.1029/2008gl037079

Horton, D. E., Johnson, N. C., Singh, D., Swain, D. L., Rajaratnam, B., & Diffenbaugh, N. S. (2015). Contribution of changes in atmospheric circulation patterns to extreme temperature trends. *Nature*, *522*(7557), 465–469. https://doi.org/10.1038/nature14550

Huang, J., Xie, Y., Guan, X., Li, D., & Ji, F. (2017). The dynamics of the warming hiatus over the Northern Hemisphere. *Climate Dynamics*, *48*(1–2), 429–446. https://doi.org/10.1007/s00382-016-3085-8

Kapsch, M., Graversen, R., & Tjernström, M. (2013). Springtime atmospheric energy transport and the control of Arctic summer sea-ice extent. *Nature Climate Change*, *3*(8), 744–748. https://doi.org/10.1038/nclimate1884

Kosaka, Y., & Xie, S. (2013). Recent global-warming hiatus tied to equatorial Pacific surface cooling. *Nature*, *501*(7467), 403–407. https://doi.org/10.1038/nature12534

Laîné, A., Yoshimori, M., & Abe-Ouchi, A. (2016). Surface Arctic amplification factors in CMIP5 models: Land and oceanic surfaces and seasonality. *Journal of Climate*, *29*(9), 3297–3316. https://doi.org/10.1175/jcli-d-15-0497.1

Liu, J., Song, M., Horton, R. M., & Hu, Y. (2013). Reducing spread in climate model projections of a September ice-free Arctic. *Proceedings of the National Academy of Sciences*, *110*(31), 12571–12576. https://doi.org/10.1073/pnas.1219716110

Lu, J., & Cai, M. (2009). Seasonality of polar surface warming amplification in climate simulations. *Geophysical Research Letters*, *36*(16), L16704. https://doi.org/10.1029/2009gl040133

Manabe, S., & Stouffer, R. J. (1980). Sensitivity of a global climate model to an increase of CO_2 concentration in the atmosphere. *Journal of Geophysical Research*, *85*(C10), 5529–5554. https://doi.org/10.1029/jc085ic10p05529

SIMIP Community (2020). Arctic sea ice in CMIP6. *Geophysical Research Letters*, *47*(10), e2019GL086749. https://doi.org/10.1029/2019gl086749

Notz, D., & Stroeve, J. (2016). Observed Arctic sea-ice loss directly follows anthropogenic CO_2 emission. *Science*, *354*(6313), 747–750. https://doi.org/10.1126/science.aag2345

Notz, D., & Stroeve, J. (2018). The trajectory towards a seasonally ice-free Arctic Ocean. *Current Climate Change Reports*, *4*, 407–416. https://doi.org/10.1007/s40641-018-0113-2

O'Neill, B. C., Kriegler, E., Ebi, K. L., Kemp-Benedict, E., Riahi, K., Rothman, D. S., et al. (2017). The roads ahead: Narratives for shared socioeconomic pathways describing world futures in the 21st century. *Global Environmental Change*, *42*, 169–180. https://doi.org/10.1016/j.gloenvcha.2015.01.004

Overland, J. E., Dethloff, K., Francis, J. A., Hall, R. J., Hanna, E., Kim, S., et al. (2016). Nonlinear response of mid-latitude weather to the changing Arctic. *Nature Climate Change*, *6*(11), 992–999. https://doi.org/10.1038/nclimate3121

Pithan, F., & Mauritsen, T. (2014). Arctic amplification dominated by temperature feedbacks in contemporary climate models. *Nature Geoscience*, *7*(3), 181–184. https://doi.org/10.1038/ngeo2071

Schneider, T., Bischoff, T., & Płotka, H. (2015). Physics of changes in synoptic midlatitude temperature variability. *Journal of Climate*, *28*(6), 2312–2331. https://doi.org/10.1175/jcli-d-14-00632.1

Screen, J. A. (2017). The missing Northern European winter cooling response to Arctic sea ice loss. *Nature Communications*, *8*(1), 14603. https://doi.org/10.1038/ncomms14603

Screen, J. A., & Simmonds, I. (2010). The central role of diminishing sea ice in recent Arctic temperature amplification. *Nature*, *464*(7293), 1334–1337. https://doi.org/10.1038/nature09051

Serreze, M. C., & Francis, J. A. (2006). The Arctic amplification debate. *Climatic Change*, *76*(3–4), 241–264. https://doi.org/10.1007/s10584-005-9017-y

Serreze, M. C., Holland, M. M., & Stroeve, J. (2007). Perspectives on the Arctic's shrinking sea-ice cover. *Science*, *315*(5818), 1533–1536. https://doi.org/10.1126/science.1139426

Smith, D. M., Screen, J. A., Deser, C., Cohen, J., Fyfe, J. C., García-Serrano, J. R., et al. (2019). The Polar Amplification Model Intercomparison Project (PAMIP) contribution to CMIP6: Investigating the causes and consequences of polar amplification. *Geoscientific Model Development*, *12*(3), 1139–1164. https://doi.org/10.5194/gmd-12-1139-2019

Steinman, B. A., Mann, M. E., & Miller, S. K. (2015). Atlantic and Pacific multidecadal oscillations and northern hemisphere temperatures. *Science*, *347*(6225), 988–991. https://doi.org/10.1126/science.1257856

Stouffer, R. J., & Manabe, S. (2017). Assessing temperature pattern projections made in 1989. *Nature Climate Change*, *7*(3), 163–165. https://doi.org/10.1038/nclimate3224

Stroeve, J. C., Kattsov, V., Barrett, A., Serreze, M., Pavlova, T., Holland, M., & Meier, W. N. (2012). Trends in Arctic sea ice extent from CMIP5, CMIP3 and observations. *Geophysical Research Letters*, *39*(16), L16502. https://doi.org/10.1029/2012gl052676

Taylor, K. E., Stouffer, R. J., & Meehl, G. A. (2012). An overview of CMIP5 and the experiment design. *Bulletin America Meteorology Social*, *93*(4), 485–498. https://doi.org/10.1175/bams-d-11-00094.1

Taylor, P. C., Cai, M., Hu, A., Meehl, J., Washington, W. M., & Zhang, G. J. (2013). A decomposition of feedback Contributions to polar warming amplification. *Journal of Climate*, *26*(18), 7023–7043. https://doi.org/10.1175/jcli-d-12-00696.1

Tsubouchi, T., Våge, K., Hansen, B., Larsen, K. M. H., Osterhus, S., Johnson, C., et al. (2021). Increased ocean heat transport into the Nordic Seas and Arctic Ocean over the period 1993–2016. *Nature Climate Change*, *11*(1), 21–26. https://doi.org/10.1038/s41558-020-00941-3

Wang, M., & Overland, J. E. (2012). A sea ice free summer Arctic within 30 years: An update from CMIP5 models. *Geophysical Research Letters*, *39*(18), L18501. https://doi.org/10.1029/2012gl052868

Wang, S., Nath, D., Chen, W., & Wang, L. (2020). Changes in winter stationary wave activity during weak mid-latitude and Arctic thermal contrast period. *International Journal of Climatology*, *40*(3), 1755–1768. https://doi.org/10.1002/joc.6299

Winton, M. (2006). Amplified Arctic climate change: What does surface albedo feedback have to do with it? *Geophysical Research Letters*, *33*(3), L03701. https://doi.org/10.1029/2005gl025244

Wu, Z., Li, X., Li, Y., & Li, Y. (2016). Potential Influence of Arctic Sea Ice to the inter-annual variations of East Asian Spring Precipitation. *Journal of Climate*, *29*(8), 2797–2813. https://doi.org/10.1175/jcli-d-15-0128.1

Xie, S., Hu, K., Hafner, J., Tokinaga, H., Du, Y., Huang, G., & Sampe, T. (2009). Indian Ocean Capacitor effect on Indo–western Pacific climate during the summer following El Niño. *Journal of Climate*, *22*(3), 730–747. https://doi.org/10.1175/2008jcli2544.1

Xie, Y., Huang, J., & Liu, Y. (2017). From accelerated warming to warming hiatus in China. *International Journal of Climatology*, *37*(4), 1758–1773. https://doi.org/10.1002/joc.4809

Xie, Y., Huang, J., & Ming, Y. (2019). Robust regional warming amplifications directly following the anthropogenic emission. *Earth's Future*, *7*(4), 363–369. https://doi.org/10.1029/2018ef001068

Xie, Y., Wu, G., Liu, Y., Huang, J., & Nie, H. (2021). A dynamic and thermodynamic coupling view of the linkages between Eurasian cooling and Arctic warming. *Climate Dynamics*, *58*(9–10), 2725–2744. https://doi.org/10.1007/s00382-021-06029-8

Yoshimori, M., Abe-Ouchi, A., & Laîné, A. (2017). The role of atmospheric heat transport and regional feedbacks in the Arctic warming at equilibrium. *Climate Dynamics*, *49*(9–10), 3457–3472. https://doi.org/10.1007/s00382-017-3523-2

Zhang, X., Sorteberg, A., Zhang, J., Gerdes, R., & Comiso, J. C. (2008). Recent radical shifts in atmospheric circulations and rapid changes in Arctic climate system. *Geophysical Research Letters*, *35*(22), L22701. https://doi.org/10.1029/2008GL035607